PCCP

PAPER

View Article Online
View Journal

Cite this: DOI: 10.1039/c5cp01852h

A novel synthetic strategy for magnetite-type compounds. A combined experimental and DFT-computational study†

Luigi Cigarini,[a] Davide Vanossi,[a] Federica Bondioli[bc] and Claudio Fontanesi*[a]

Received 30th March 2015,
Accepted 6th July 2015

DOI: 10.1039/c5cp01852h

www.rsc.org/pccp

The dynamics of the early stage reaction between benzyl alcohol and Fe(acetylacetonate)$_3$ is studied by exploiting the Dynamic Reaction Coordinate (DRC) approach, at the PBE0/6-31G* level of theory. Analysis of the DRC trajectory provides a detailed molecular insight into the catalytic effect observed in the acidic reaction environment, compared to the neutral one. The presence of an additional proton in the reaction system, meant to simulate an acidic reaction environment, dramatically affects the reaction path: both by decreasing the activation energy of the complex dissociation and leading to the formation of acetone.

1. Introduction

One of the most powerful preparation routes towards metal oxide nanocrystals is represented by non-hydrolytic sol–gel (NHSG) synthesis in an organic solvent. This method permits to overcome some of the major limitations of traditional aqueous sol–gel chemistry, such as poor reproducibility of the synthesis protocols and low crystallinity degree of the product.[1] In non-aqueous colloidal sol–gel chemistry the transformation of the precursor species (inorganic metal salts, alkoxides, acetates and acetylacetonates) into the oxidic compound takes place in an organic solvent, which acts as a reactant as well as a control agent for particle growth, allowing the synthesis of high purity nanomaterials in surfactant-free reaction mixtures.[2] For the hydrolytic sol–gel synthesis, NHSG is divided into two steps. The first step involves the reaction of a metal halide, a metal alkoxide, acetates or acetylacetonates with an organic oxygen donor (such as alcohols, ethers, or glycols). The second step (condensation) can follow different pathways depending on the alkoxide employed. One of the most used condensation reactions occurs through alkyl halide elimination and/or ether elimination as schematically indicated:[3]

$$\text{Step 1}\quad MX_m + n\text{ROH} \rightarrow M(X)_{m-n}(OR)_n + n\text{HX}$$

$$\text{Step 2}\quad \equiv M-OR + RO-M \equiv \rightarrow \equiv M-O-M \equiv + R-O-R$$

$$\text{and/or}\quad \equiv M-OR + X-M \equiv \rightarrow \equiv M-O-M \equiv + R-X$$

Pinna[4] *et al.* were the first to report the synthesis of nanocrystalline magnetite particles starting from iron(III) acetylacetonate and using only benzyl alcohol (BzOH) as a solvent and a ligand at the same time. Following this first experimental work, Niederberger[3] proposed the reaction scheme (Fig. 1). The analysis of the organic species in the final synthesis liquid revealed that in fact the reaction commences with a solvolysis of the acetylacetonate species, followed by aldol or ketimine condensation reactions. Benzyl alcohol nucleophilically attacks one carbonyl group of the acetylacetonate ligand. Alcoholysis leads to benzyl acetate and an enolate ligand. In a next step, benzyl alcohol coordinates to the Fe center, releasing benzyl acetate in a ligand exchange reaction. Then, the enolate attacks the coordinated benzyl alkoxide, and 4-phenyl-2-butanone is released. The Fe-bound hydroxyl group binds to another Fe center, representing the starting point of nanoparticle formation. A number of side products were also identified in the final reaction mixture. 4-Phenyl-3-buten-2-one, which was found in small amounts, is an oxidation product of 4-phenyl-2-butanone. Starting from FeIII, one third of the iron must be reduced to FeII to obtain phase-pure magnetite. Therefore, 4-phenyl-3-buten-2-one is proposed to be formed from 4-phenyl-2-butanone by dehydrogenative oxidation, concurrently reducing two iron centres, which means that in principle the benzyl alcohol solvent leads to the partial reduction of iron and provides for the correct stoichiometry of the oxide product.

Following these studies, Bondioli *et al.*[5] also evaluated the effect of tionyl chloride, $SOCl_2$, as a catalyser, considering also the effect of synthesis parameters (time and temperature) on the physical and magnetic properties of the so-obtained powder. The use of $SOCl_2$ allowed us to obtain pure magnetite nanoparticles in a shorter time; however, as in the case of the samples obtained without the catalyser, the powders prepared with a synthesis

[a] University of Modena and Reggio Emilia, DSCG, Via G. Campi 41125, Modena, Italy. E-mail: claudio.fontanesi@unimore.it
[b] Department of Industrial Engineering, University of Parma, Viale Parco Area delle Scienze, 181/A, 43124 Parma, Italy
[c] Consorzio INSTM, Via G. Giusti 9, 51121 Firenze, Italy

† Electronic supplementary information (ESI) available. See DOI: 10.1039/c5cp01852h

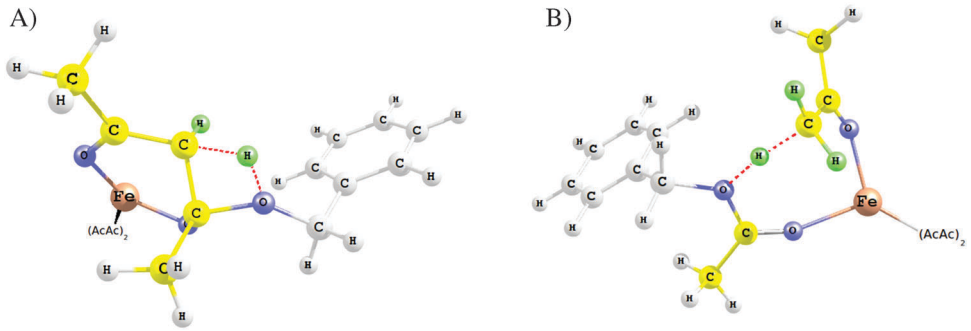

Fig. 1 (A) Transition state neutral (TSN). (B) Transition state acid (TSA).

time of 8 h appear to have slightly enhanced magnetic properties (higher saturation magnetization and higher coercive field) with respect to those prepared with similar (both shorter and longer) synthesis times.[5,6] The aim of this work is to rationalize theoretically the synthetic reaction path, with a focus on the role played by the acidity of the reactive medium. In particular, the initial attack of a benzyl alcohol molecule on the $Fe(acac)_3$ complex was analysed considering a number of different reciprocal orientations, to shed light on the early stage of the reaction path, the latter is described in detail in the following section, at a molecular level. In this work, the synthesis of magnetic iron oxide nanoparticles (MNPs) by the NHSG route was evaluated by exploiting the DRC method (a classical molecular dynamics study relying on an *ab initio*/DFT based hypersurface) in order to better define the reaction mechanism.

2. Experimental reactivity

The early stages, in the reaction between $Fe(acac)_3$ and benzyl alcohol, are indicated to play a major role.[3,4] Thus, on the basis of the experimental results present in the literature the following reaction elementary steps are considered.

Chart 1a shows that the first step is a nucleophilic attack by a solvent molecule (circled in blue in the figure) to the electrophilic site of the substrate, typical of sol–gel processes.[3] Then this attack leads, with the involvement of a second molecule of solvent (circled in red), to the breakdown of the acetylacetonate conjugated system, Chart 1b, allowing a ligand substitution reaction, Chart 1c, on the central iron atom. In which a solvent molecule (circled in green) substitutes the acetylacetonate fragment, and the latter has previously been attacked in the first step. In a six-centre mechanism, the oxydrilic group previously on the solvent molecule ends up on the iron atom, and a 4-phenyl-2-propanone molecule (circled in green – carrying the phenyl previously on the solvent molecule) and the residual part of the acetylacetonate moiety separate from the substrate complex, Chart 1d. It is thought that the two remaining acetylacetonate moieties, yet bound to the iron atom, follow the same reaction mechanism (the solvolysis part of the sol–gel mechanism). Then, the residual iron(III) hydroxide, Chart 1e, undergoes the condensation step, eventually yielding the magnetite lattice, Chart 1f.

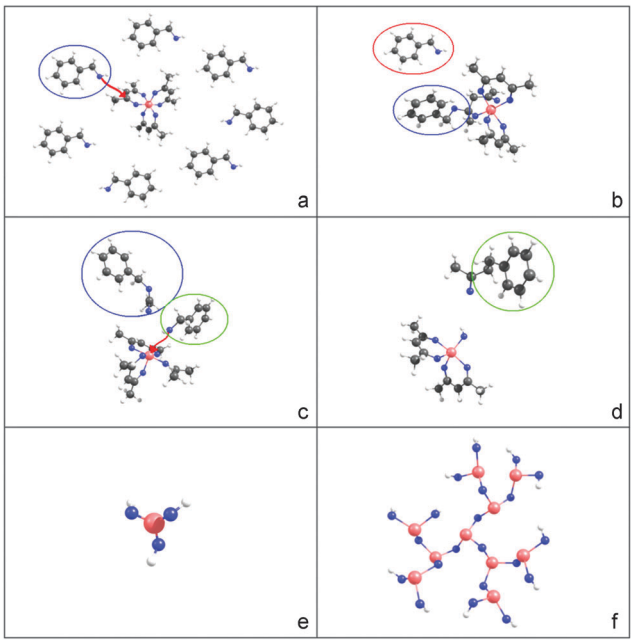

Chart 1 Main reaction occurring upon NHSG treatment of $Fe(AcAc)_3$ in benzyl alcohol.

3. Calculation details

In the present work the overall calculations were performed in the framework of *ab initio* methods using Firefly QC package,[7] which is partially based on the GAMESS (US)[8] source code. If otherwise indicated, all the calculations were performed using C_1 symmetry and are of U-DFT type. The results here presented are obtained by using the PBE0 hybrid functional. In order to gain confidence about the reliability of the results, we chose the all-electron split valence plus polarization basis set 6-31G*. Several preliminary test calculations were also carried out using the B3LYP functional and smaller basis sets: LanL2DZ, 3-21G* and the generalized mixed ECP 6-31G*. IR spectra obtained at the PBE0/6-31G* level of the theory showed an extremely good agreement with the experimental results (details about the comparison between experimental and theoretical spectra can be found in the ESI†). It must be noted that a "good" quality in the calculation of the vibrational spectrum is needed, as a reference, because the search of reaction steady states (transition states

and intermediate complex states) is based on a reliable Hessian analysis. The question of spin multiplicity has been addressed by comparing results obtained by calculations performed with 2, 4, and 6 multiplicities. Lower values in energy are systematically obtained for the sextet, while the quartet shows great convergence problems. In particular a tight comparison of transition state structure, electronic configuration and Hessian analysis is performed in the case of the protonated TS. Despite the large difference in total energy, the sextet electronic configuration is found to be about 15 kcal mol^{-1} more stable than the doublet, the differences in both Hessian analysis and TS geometries are negligible, and details can be found in the ESI.† In fact, DRC curves of the multiplicity 2 and 6 show a quite similar energy *vs.* time pattern in both the qualitative trend and the quantitative amplitude of energy oscillations, compare R&D Section 4.2, thus once the initial energy is normalized to zero, no substantial differences are found both quantitatively and qualitatively on the energy *vs.* time reaction trajectory. Thus, in the following the major part of the results (DRC trajectories) are calculated for the doublet state, even if for both the neutral and protonated systems at least one DRC trajectory has been calculated also for the sextet.

4. Results and discussion

4.1 Reaction path

The benzyl alcohol molecule initial attack on the $Fe(acac)_3$ complex was analysed by considering a number of different reciprocal orientations. Fig. 1 shows the structure of two transition states obtained for the neutral (TSN) and protonated systems (TSA).

Fig. 2 shows the structure of the entry and exit complexes and Fig. 3 shows the relevant energy *vs.* reaction coordinate plot, both for the neutral and protonated cases: top left and right two graphs show multiplicity 2 results, and top left and right two graphs show multiplicity 6 results. Negligible geometrical differences are found in the R, ECA, TSA, and ESA structures when comparing 2 and 6 multiplicity results (compare also the multiplicity 2 and 6 DRC results). The main difference concerns the activation energy: 6.59 and 43.45 kcal mol^{-1} for multiplicity 2 and 6, respectively. Thus, multiplicity 2 seems to better account for the greater experimental yield and speed of reaction found in the acidic environment. For this greater attention was devoted to a systematic study of the multiplicity 2 system, *i.e.* DRC calculations. The transition state in the neutral environment (TSN) features an almost unaffected geometry with respect to the acetylacetonate complex. In contrast, the acidic environment homologous transition state structures (TSA) are characterized by a dramatic increase in the carbon–carbon bond distances involved in the co-ordinate (dative covalent) bond. In TSN the distance between the two carbon atoms of the acetylacetonate moiety, that is the bonds which are known experimentally to dissociate in the reaction, is about 1.53 Å, yet in the range of a single C–C bond distance, and in TSA the corresponding C–C distance is about 3.52 Å. Notably, the O–Fe–O angle is just wider in TSN (95.2°) than in TSA (93.5°): the increases in distances between the two oxygens and between the two carbons mentioned before are not related to the spread of this angle (which shrinks instead) but it is due to an increase in the distance of iron–oxygen on the side on which the solvent attacks: this distance is 1.90 Å on TSN, but it reaches 2.08 Å on TSA. So, the comparison of the TSN and TSA main geometrical parameters allows us to infer that for the reaction in acidic medium (TSA), the first leaving moiety is probably the one derived from the side attacked by the solvent: the iron–oxygen bond distances, indeed, are 1.95 Å on the not attacked side and 2.08 Å on the attacked side. This is not so evident in neutral medium (TSN): here the iron–oxygen distances are 2.00 Å on the not attacked side and 1.90 Å on the solvent attacked side. On the whole, the comparison of the TSA and TSN geometries shows that the process appears to be a more sterically hindered structure for TSN than for TSA.

Fig. 2 shows exit complex structures, and neutral (ECN) and acidic (ECA) media, obtained following full optimizations starting from the transition states. Very interestingly, even at this stage, the structure derived from the reaction in a neutral environment presents its acetylacetonate chain almost intact. Whilst, ECA features the presence of a well defined acetone moiety, the upper part of Fig. 2B.

In ECA, the distance between the two carbon atoms, previously part of the acetylacetonate moiety, has increased to 3.60 Å, while in ECN it remains almost the same as in the TSN.

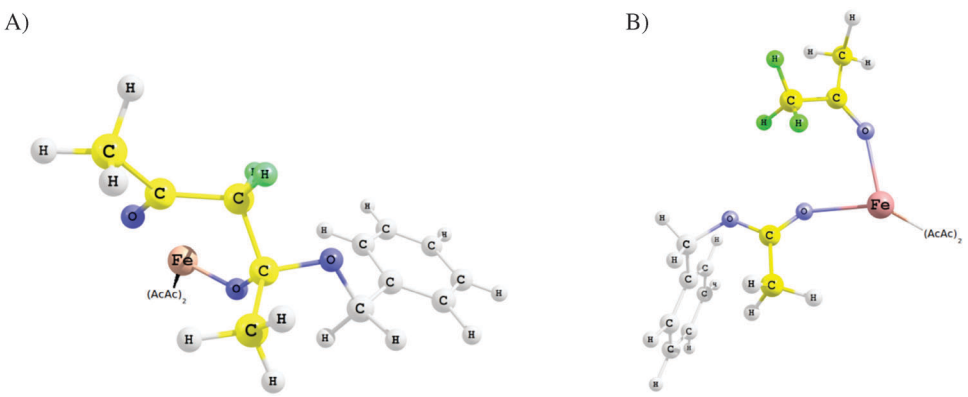

Fig. 2 (A) Exit complex neutral (ECN). (B) Exit complex acid (ECA).

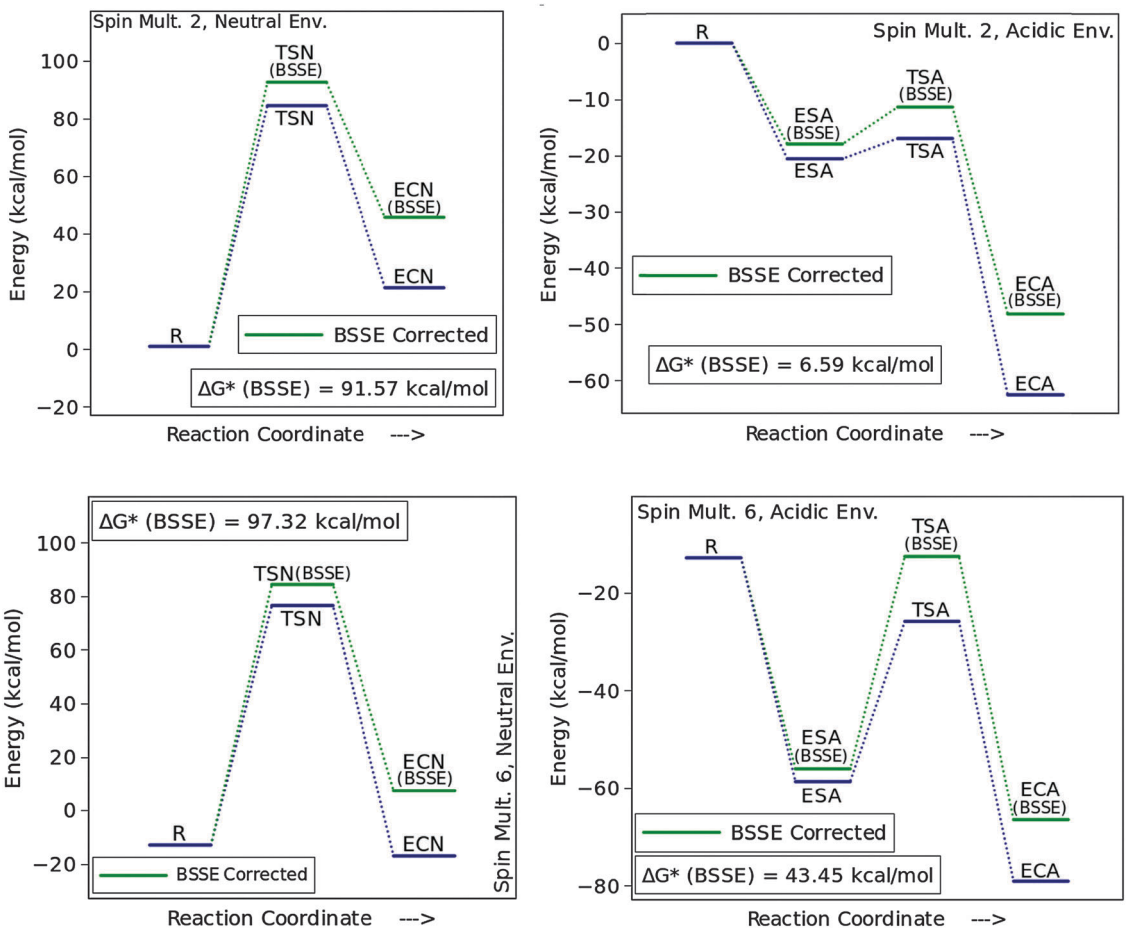

Fig. 3 Energy *vs.* reaction coordinate pattern. Top left: Spin multiplicity 2, neutral environment. Top right: Spin multiplicity 2, acidic environment. Bottom left: Spin multiplicity 6, neutral environment. Top right: Spin multiplicity 6, acidic environment.

In ECA, both the iron–oxygen bonds of the acetylacetonate chain interested in the reaction measure approximately the same length, which are around 2.1 Å (a larger value with respect to the equilibrium 1.99 Å one). In ECN shorter Fe–O distances, 1.85 Å, are found on the side involved in the benzaldehyde attack, while larger Fe–O distances, about 2.20 Å, are found on the side interested by the entering solvent. Indeed, the electron density distribution shows a great increment of electronic density near to the central carbon of the chain under attack and in TSA a Mulliken charge of −0.714 is found on this carbon, while on TSN this value is −0.617. Various attempts to find any entrance complex have been performed both in neutral and acidic systems. This led us to the convincement that no entrance complex is present in the two studied reaction paths. Only something similar to it has been found in the simulated acidic medium system. We called this Entrance State Acid (ESA) for the simple reason that it is not a complex: the two reagents are still separated in it. The transfer of the acidic proton from the solvent to the acetylacetonate complex leads to a stationary point, the ESA, where there is no chemical interaction between the resulting two species, but smaller forces between them regulate the geometric configuration. ESA's electronic energy is about 20 kcal mol^{-1} lower than the sum of reagent's energy at

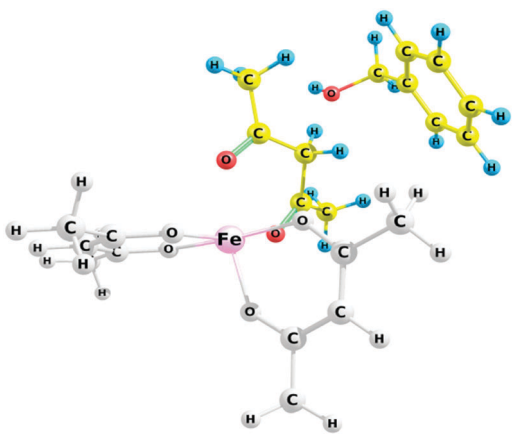

Fig. 4 Entrance state acid (ESA).

spin multiplicity 2 and about 45 kcal mol^{-1} lower than that of reagents at spin multiplicity 6. ESA is shown in Fig. 4.

4.2 Classical reaction dynamics on a PBE0/6-31G* energy hyper-surface (DRC)

TS structures represented in Fig. 1, and the relevant electronic properties, are exploited for building up suitable initial conditions

in terms of spatial coordinates and velocity vectors, to run dynamic reaction coordinate molecular dynamics calculations.[9,10] We report results for six different DRC runs: four of them in the acidic medium (*i.e.* starting from TSA) and two runs carried out in the neutral medium (*i.e.* starting from the TSN). The DRC trajectory is specified by assigning an arbitrary kinetic energy to all the TS frequency normal modes minus one, in fact we assigned the reaction coordinate, *i.e.* the one

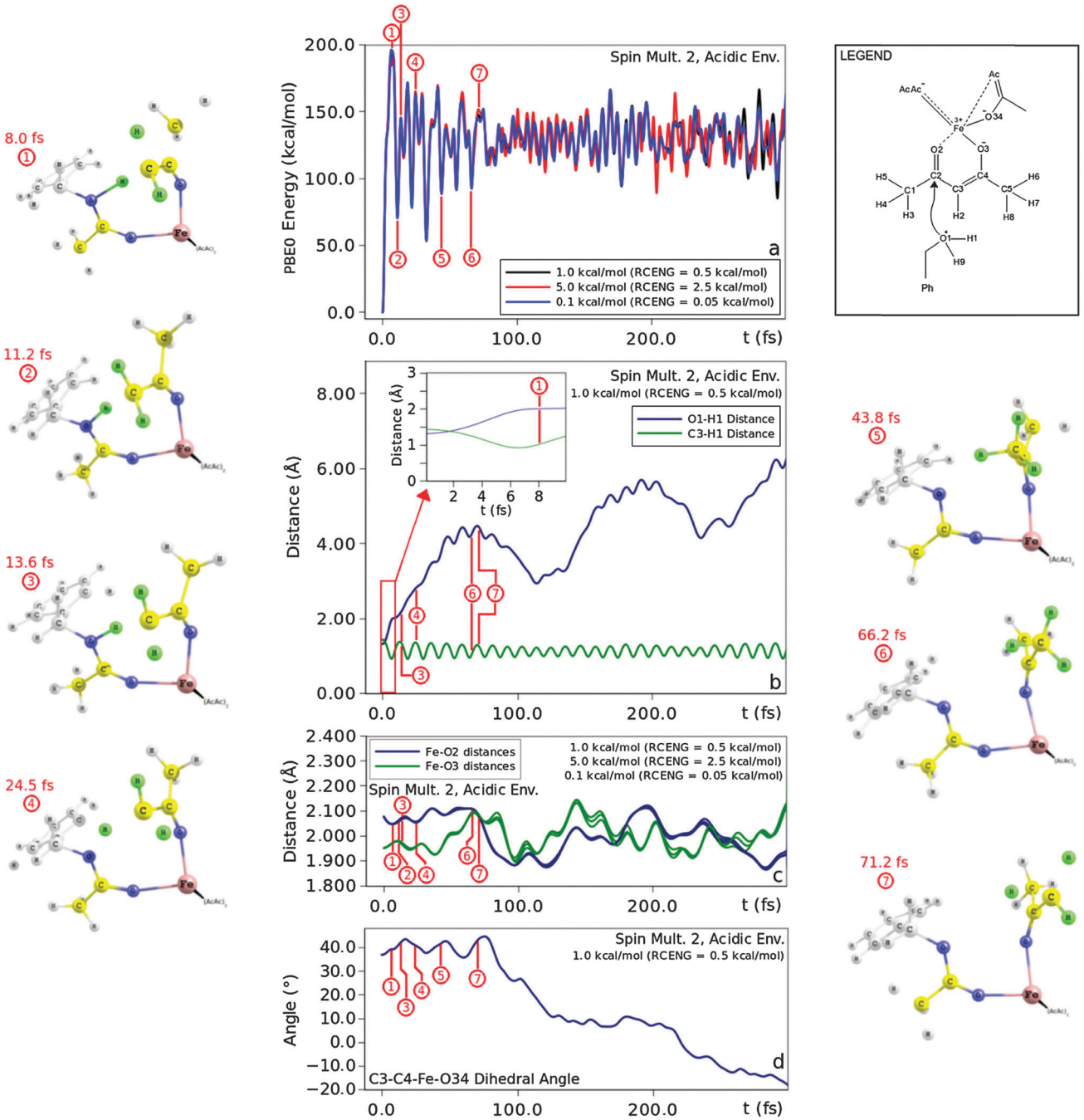

Fig. 5 (a) PBE0 electronic energy (potential energy) as a function of simulated time for three different DRC calculations, all starting from TSA and performed with an imposed electron spin multiplicity of 2. The three calculations differ from each other for the total nuclear kinetic energy distributed to the system at the start, and for the amount of this (RCENG) attributed to the intrinsic reaction coordinate. (b) Two different geometrical parameters of the system (O–H and C–H bond lengths involved in the reaction) plotted as a function of simulated time for one of the same DRC calculations above-mentioned. (c) Evolution of other two different geometrical parameters (Fe–O bond lengths involved in the reaction) during the simulated time of the same three calculations. (d) From one of the same DRC calculations: evolution of a dihedral angle involved in the reaction which evidently clears the moving away of C3 carbon (see legend) from the reaction centre, due to a rotatory movement of the ''acetone'' residue, after the break of the O–H bond. (Left and right) Seven graphical representations of the system (nuclear spatial positions) at different simulated times for one of the DRC calculations above-mentioned: 5.0 kcal mol^{-1}, RCENG = 2.5 kcal mol^{-1}.

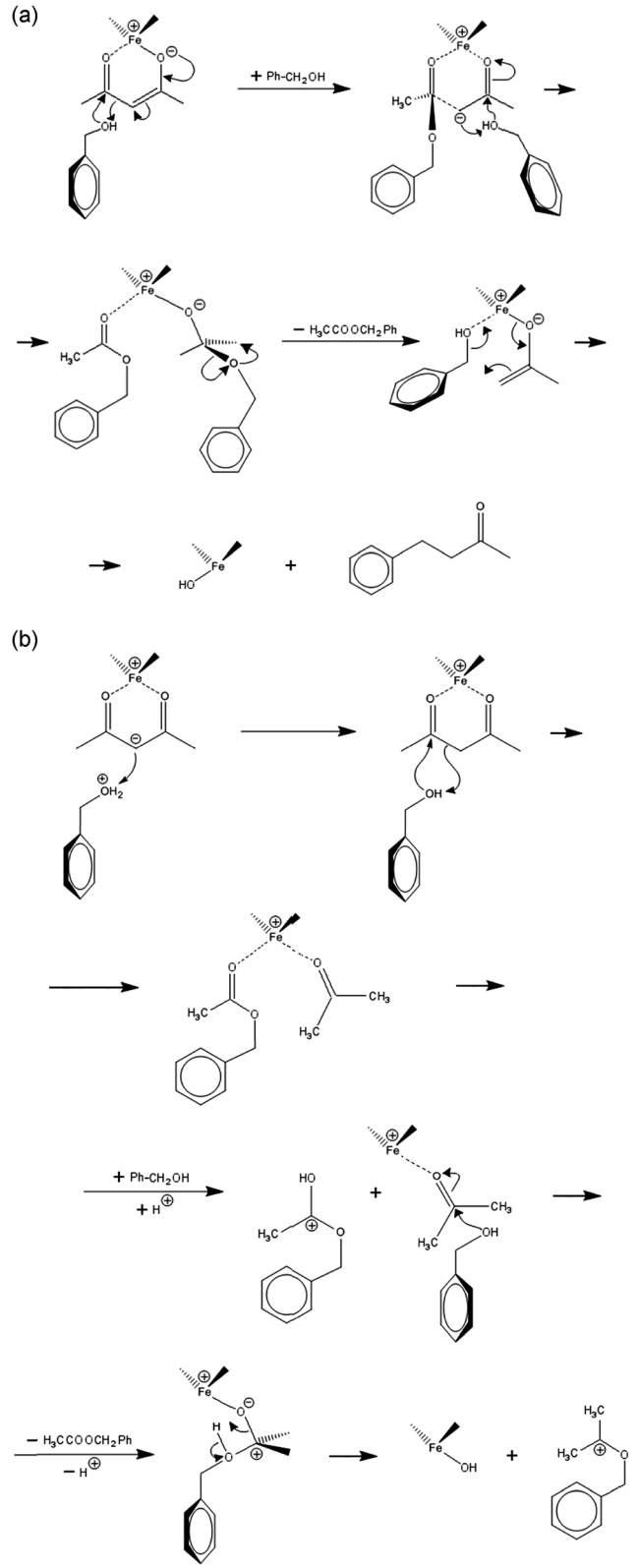

Chart 2 (a) Neutral mechanism. (b) Acidic medium mechanism.

corresponding to the TS imaginary frequency normal mode.[11–13] Using the Hessian matrix calculated for TSA and TSN, we set up different initial velocity vectors: $\nu 1$ (0.1 and 0.05 kcal mol^{-1}), $\nu 2$ (1.0 and 0.5 kcal mol^{-1}), and $\nu 3$ (5.0 and 2.5 kcal mol^{-1}), where the first value of energy is the value assigned as total kinetic energy and the second energy value is assigned specifically to the reaction coordinate mode. For TSA DRC calculations were carried out with multiplicity = 2 with $\nu 1$, $\nu 2$ and $\nu 3$ initial velocity vectors and multiplicity = 6 only using the $\nu 2$ initial velocity vector. Fig. 5 shows the details concerning the three simulations with multiplicity = 2. Two DRC calculations have been carried out starting from TSN, both using $\nu 2$ as the initial velocity vector, with spin multiplicity 2 and 6 (the results are reported in the ESI†). The results of DRC trajectories are graphically presented in a variety of ways: showing the total electronic energy of the system as a function of the simulated time (Fig. 1A), as well as showing the variation of a number of selected geometrical parameters of the system over the simulation time. Fig. 5a is characterized by large oscillations in energy up to 80 fs, note that after 8 fs (structure 1 in the left panel) the C3–H1 bond goes through a minimum and the relevant CH_3 moiety (leading to the acetone formation) is formed: Fig. 5b compares the variation of the C3–H1 (green line) and O1–H1 (blue line) bond distances as a function of time, the C3–H1 distance oscillates about 1.1 Å, whilst the O1–H1 distance increases monotonically. Structures 2 through 5, time spans between 8 and 44 fs, are characterized by the definitive transfer of the "acidic" hydrogen from the protonated benzaldehyde and the CH_3 group stabilization, and structures 6 and 7 show the variation of the dihedral angle and the rotation of the acetone molecule in a position suitable to leave the iron complex. Compare the increase in the Fe–O3 bond distance at about 250 fs with respect to the Fe–O2 one (Fig. 5c), as well as the 160 degree variation of the C3–C4–Fe–O34 dihedral angle (Fig. 5d). All in all, our theoretical results taken together with the results in the literature allow us to propose two different mechanisms, neutral and acidic media, as depicted in Chart 2a and b. Fig. 6 shows the details concerning the simulation with multiplicity = 6. The energy pattern closely resembles the one obtained in the case of multiplicity = 2 (Fig. 5). What is more, also the structural evolution of the reaction with multiplicity 6 closely resembles the global outcome obtain with multiplicity = 2 (acetone is the final exiting product of the reaction between iron acetylacetonate and benzaldehyde).

5. Conclusions

The theoretical analysis allows us to shed light on the reaction mechanism at a molecular level. In particular, both the steady state and dynamic evidence concur to obtain a self-consistent picture.

(i) The steady state reaction path, in terms of energy levels, shows that the presence of an additional proton, *i.e.* the acidic environment, causes a substantial decrease, about 85 kcal mol^{-1}, in the activation energy: 92 kcal mol^{-1} and 7 kcal mol^{-1} for the neutral and acidic environment, respectively, compare the energy reaction path shown in Fig. 3.

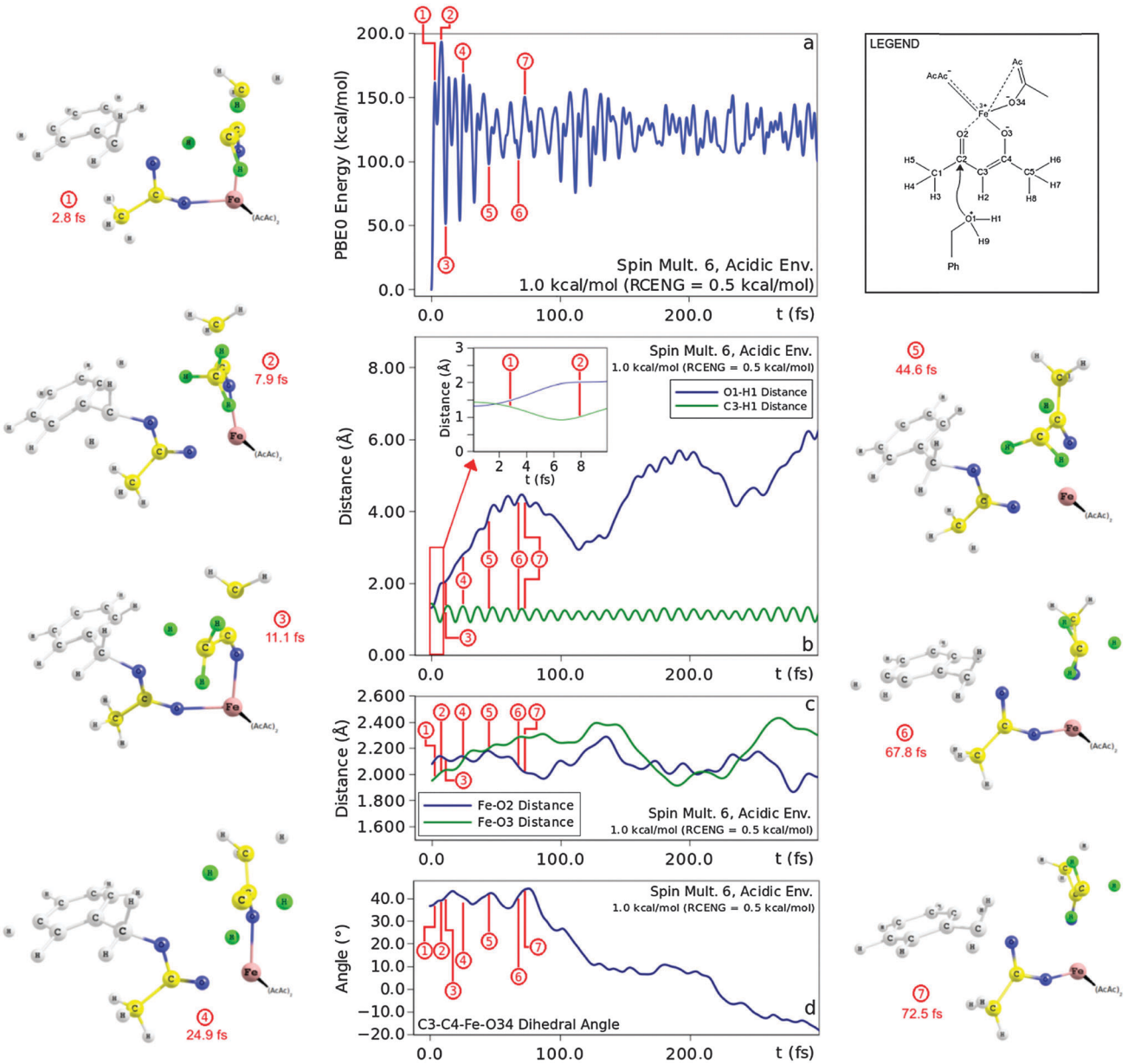

Fig. 6 (a) PBE0 electronic energy (potential energy) as a function of simulated time for three different DRC calculations, all starting from TSA and performed with an imposed electron spin multiplicity of 6. Total kinetic energy 1 kcal mol^{-1} distributed to the whole system at the start, RCENG = 0.5 kcal mol^{-1} assigned to the intrinsic reaction coordinate. (b) Two different geometrical parameters of the system (O–H and C–H bond lengths involved in the reaction) plotted as a function of simulated time for one of the same DRC calculations above-mentioned. (c) Evolution of other two different geometrical parameters (Fe–O bond lengths involved in the reaction) during the simulated time. (d) Time evolution of a dihedral angle involved in the reaction which evidently clears the moving away of C3 carbon (see legend) from the reaction centre, due to a rotatory movement of the ''acetone'' residue, after the break of the O–H bond. (Left and right) Seven graphical representations are shown of the system (nuclear spatial positions) at different simulation times.

(ii) A detailed analysis of the DRC trajectory shows that the additional proton, acidic environment, allows for the formation of an acetone molecule, which leads both to the formation of a neutral molecule which is a suitable ''leaving group'' as a major step in the $Fe(acac)_3$ complex degradation. Indeed this result is also quantitatively heralded by the longer, weaker Fe–O (forming acetone) distance, in comparison to the behaviour of the ''neutral'' system: compare Fe–O2 and Fe–O3 distance *vs.* time patterns in Fig. 5c.

Thus, the DRC analysis allows for a reliable quantitative analysis of the reaction path. A feature which can be definitively exploited in view of a prevision of the reaction path when dealing with such a class of reactions, see for example ref. 13–19.

Acknowledgements

Consorzio INSTM is gratefully acknowledged.

References

1 J. Livage, M. Henry and C. Sanchez, *Prog. Solid State Chem.*, 1988, **18**, 259–341.
2 N. Pinna and M. Niederberger, *Angew. Chem., Int. Ed.*, 2008, **47**, 5292–5304.
3 M. Niederberger and G. Garnweitner, *Chem. – Eur. J.*, 2006, **12**, 7282–7302.
4 N. Pinna, S. Grancharov, P. Beato, P. Bonville, M. Antonietti and M. Niederberger, *Chem. Mater.*, 2005, **17**, 3044–3049.
5 N. Florini, G. Barrera, P. Tiberto, P. Allia and F. Bondioli, *J. Am. Ceram. Soc.*, 2013, **96**, 3169–3175.
6 M. Sangermano, P. Allia, P. Tiberto, G. Barrera, F. Bondioli, N. Florini and M. Messori, *Macromol. Chem. Phys.*, 2013, **214**, 508–516.
7 A. A. Granovsky, Firefly version 8, http://classic.chem.msu.su/gran/firefly/index.html.
8 M. W. Schmidt, K. K. Baldridge, J. A. Boatz, S. T. Elbert, M. S. Gordon, J. H. Jensen, S. Koseki, N. Matsunaga, K. A. Nguyen, S. Su, T. L. Windus, M. Dupuis and J. A. Montgomery, *J. Comput. Chem.*, 1993, **14**, 1347–1363.
9 J. J. P. Stewart, L. P. Davis and L. W. Burggraf, *J. Comput. Chem.*, 1987, **8**, 1117–1123.
10 K. M. Dieter and J. J. P. Stewart, *THEOCHEM*, 1988, **163**, 143–149.
11 C. Fontanesi, *THEOCHEM*, 1997, **392**, 87–94.
12 C. Fontanesi, P. Baraldi and M. Marcaccio, *THEOCHEM*, 2001, **548**, 13–20.
13 C. Fontanesi, C. A. Bortolotti, D. Vanossi and M. Marcaccio, *J. Phys. Chem. A*, 2011, **115**, 11715–11722.
14 T. Taketsugu and M. S. Gordon, *J. Phys. Chem.*, 1995, **99**, 8462–8471.
15 A. Hellweg, *J. Comput. Chem.*, 2013, **34**, 1835–1841.
16 R. Spezia, C. Zazza, A. Palma, A. Amadei and M. Aschi, *J. Phys. Chem. A*, 2004, **108**, 6763–6770.
17 M. Kayanuma, T. Taketsugu and K. Ishii, *Theor. Chem. Acc.*, 2007, **120**, 191–198.
18 T. Fujiwara, H. Mori, Y. Mochizuki, H. Tatewaki and E. Miyoshi, *THEOCHEM*, 2010, **949**, 28–35.
19 H.-R. Tao and D.-C. Fang, *Theor. Chem. Acc.*, 2008, **121**, 91–101.

